

# Organic & Biomolecular Chemistry

Accepted Manuscript



This is an *Accepted Manuscript*, which has been through the Royal Society of Chemistry peer review process and has been accepted for publication.

*Accepted Manuscripts* are published online shortly after acceptance, before technical editing, formatting and proof reading. Using this free service, authors can make their results available to the community, in citable form, before we publish the edited article. We will replace this *Accepted Manuscript* with the edited and formatted *Advance Article* as soon as it is available.

You can find more information about *Accepted Manuscripts* in the [Information for Authors](#).

Please note that technical editing may introduce minor changes to the text and/or graphics, which may alter content. The journal's standard [Terms & Conditions](#) and the [Ethical guidelines](#) still apply. In no event shall the Royal Society of Chemistry be held responsible for any errors or omissions in this *Accepted Manuscript* or any consequences arising from the use of any information it contains.



Journal Name

ARTICLE

## 1,8-Bis(phenylethynyl)anthracene – gas and solid phase structures

Jan-Hendrik Lamm,<sup>a,†</sup> Jan Horstmann,<sup>a,†</sup> Hans-Georg Stammer,<sup>a</sup> Norbert W. Mitzel,<sup>a\*</sup> Yuriy A. Zhabanov,<sup>a,b</sup> Natalya V. Tverdova,<sup>b</sup> Arseniy A. Otyotov,<sup>b</sup> Nina I. Giricheva<sup>c</sup> and Georgiy V. Girichev<sup>b\*</sup>

Received 00th January 20xx,  
Accepted 00th January 20xx

DOI: 10.1039/x0xx00000x

www.rsc.org/

1,8-Bis(phenylethynyl)anthracene (1,8-BPEA) was synthesized by a twofold Kumada cross-coupling reaction. The molecular structure of 1,8-BPEA was determined using a combination of gas-phase electron diffraction (GED), mass spectrometry (MS), quantum chemical calculations (QC) and single-crystal X-ray diffraction (XRD). Five rotamers of the molecule with different orientations of phenylethynyl groups were investigated by DFT calculations. According to these molecules of  $C_2$  symmetry with co-directional rotation of the phenylethynyl groups are predicted to exist in the gas phase at 498 K. This was confirmed by a GED/MS experiment at this temperature. The bonding of this conformer was studied and described in the terms of an NBO-analysis. Dispersion interactions in the solid state structure and in the free molecule are discussed. In the solid this symmetry is broken; the asymmetric unit of the single crystal contains 3.5 molecules and a herringbone packing motif of  $\pi$ -stacked dimers and trimers. The  $\pi$ -stacking in the dimers is between the anthracene units, the trimers are linked by  $\pi$ -stacking between phenyl and anthracene units. The interaction between these stacks can be described in terms of  $\sigma(C-H)\cdots\pi$  interactions.

### Introduction

Anthracene is an important representative of polycyclic aromatic hydrocarbons and has been intensely investigated due to its applications in electronic and optoelectronic industries and in the organic semiconductor area.<sup>1,2</sup> Anthracene derivatives are promising candidates for further search of new materials with useful properties. For example, molecules based on the 9,10-bis(phenylethynyl)anthracene (9,10-BPEA) possess interesting fluorescent properties making them useful as a sensitizer in chemiluminescent devices,<sup>3</sup> as dopant in organic light emitting diodes,<sup>4,5</sup> as fluorescent dyes for biosensors<sup>6,7</sup> etc. Recently, new substituted anthracenes [polyalkynylanthracenes: bis- and tris(trimethylsilyl)ethynyl anthracenes, bis- and tris(trimethylstannyl)ethynyl anthracenes] were synthesized and completely characterized by multinuclear NMR spectroscopy, mass spectrometry as well as by X-ray diffraction (XRD) experiments.<sup>8</sup> Like the parent anthracene, these compounds undergo photodimerisation reactions upon UV irradiation. Besides these properties and applications we became interested in alkynylanthracenes because they can form rigid backbones to place certain functions in close proximity and defined orientation. We recently reported for instance the application of 1,8-

bis(diethylgallylethynyl)anthracene as a bidentate Lewis acid,<sup>9</sup> but also derivatives with aluminum and indium.<sup>10</sup>

1,8-Bis(phenylethynyl)anthracene (1,8-BPEA)<sup>11</sup> carries two benzene rings in close proximity to one another. A number of theoretical and experimental studies have been devoted to the determination of interaction between benzene rings, the most basic example being the structure of benzene dimer.<sup>12–16</sup> Early experimental measurements suggested the existence of a T-shaped structure, as the benzene dimer has a dipole moment.<sup>17,18</sup> However, studies by microwave spectroscopy<sup>18–20</sup> could not rule out the existence of other stable isomeric structures such as sandwich or parallel-displaced structures for this dimer as these configurations do not exhibit a permanent dipole moment. Dispersion (as compared with electrostatic, induction and exchange-repulsion interactions) was shown to make the dominant stabilizing contribution to the total binding energy.<sup>21</sup>

The two phenyl rings of the 1,8-BPEA molecule resemble a benzene dimer in some sense. At the same time unlike the benzene dimer, the relative orientation of these rings is restricted by the rigid anthracene skeleton. Therefore it became desirable to investigate the relative orientation of the phenyl rings in the case of 1,8-BPEA. Another question is what kind of interaction mainly stabilizes the experimentally observed geometry of the molecule. Since in the benzene dimer dispersive interactions play the dominant role we tried to estimate their contribution to the stabilization of the geometry of 1,8-BPEA utilizing DFT-D2<sup>22</sup> and DFT-D3<sup>23</sup> calculations.

This contribution focusses on the three key themes: a) a study of 1,8-BPEA in the crystalline state (intermolecular interactions); b) a theoretical and experimental investigation of free 1,8-BPEA molecule (QC and GED/MS); c) a consideration of the main interactions stabilizing the structure of 1,8-BPEA.

<sup>a</sup> Universität Bielefeld, Fakultät für Chemie, Lehrstuhl für Anorganische Chemie und Strukturchemie, Centre for Molecular Materials CM<sub>2</sub>, Universitätsstraße 25, D-33615 Bielefeld, Germany.

E-Mail: mitzel@uni-bielefeld.de; Fax: +49 521 106 6026; Tel: +49 521 106 6128.

<sup>b</sup> Ivanovo State University of Chemistry and Technology, Ivanovo 153000, Russia.

E-Mail: girichev@isuct.ru; Fax: +7 4932 417995; Tel: +7 4932 359874.

<sup>c</sup> Ivanovo State University, Ivanovo 153025, Russia.

† These authors contributed equally to this work.

Electronic Supplementary Information (ESI) available:

See DOI: 10.1039/x0xx00000x

## Results and discussion

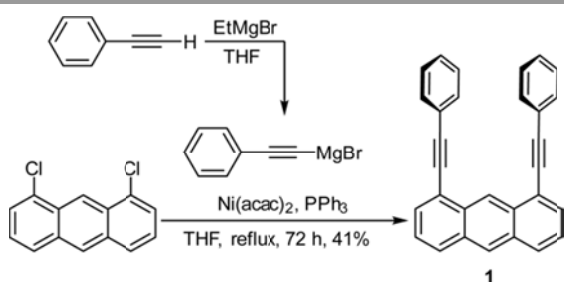
### Synthesis and characterization of 1,8-BPEA

In analogy to literature protocols,<sup>8,24</sup> 1,8-BPEA (**1**) was synthesized by a twofold Kumada cross-coupling reaction, using 1,8-dichloroanthracene and (phenylethynyl)magnesium bromide, which was freshly prepared by conversion of phenylacetylene with ethylmagnesium bromide (Scheme 1).

After column chromatography, the product was obtained in the form of bright yellow crystals and was identified by multi-nuclear NMR spectroscopy as well as (high resolution) mass spectrometry. The <sup>1</sup>H NMR spectra show typical patterns for 1,8-substituted anthracenes consisting of two singlets for the protons in positions 9 and 10, two doublets for H2/H7 and H4/H5, respectively, as well as one doublet of doublets for H3/H6 (for NMR spectroscopic assignments see Scheme 2). The <sup>13</sup>C NMR spectrum of 1,8-BPEA shows the anticipated number of resonances.

### Quantum-chemical calculations

1,8-BPEA was studied as a single molecule using various DFT functionals: B3LYP, CAM-B3LYP, LC-BLYP, LC-wPBE, M06<sup>25</sup> with



Scheme 1 Synthesis of 1,8-BPEA (**1**).

cc-pVTZ<sup>26</sup> basis sets. The dispersion interaction in free molecule 1,8-BPEA was studied using the dispersion corrected DFT methods B3LYP-D2/cc-pVTZ and B3LYP-D3/cc-pVTZ. The molecular geometry of 1,8-BPEA was optimized starting with structures of different symmetries. The explored models differ by the orientation of the phenyl fragments. Transitions between models can be realized by rotation of the phenylethynyl groups. Structural models of the 1,8-BPEA molecule (Fig. 1) are as follows:

- model 1 ( $C_{2v}$  symmetry): both phenyl fragments are located in the anthracene plane;
- model 2 ( $C_s$  symmetry): one phenyl fragment is located in the anthracene plane and the other is perpendicular to the anthracene skeleton;
- model 3 ( $C_{2v}$  symmetry): both phenyl fragments are perpendicular to the anthracene plane;
- model 4 ( $C_2$  symmetry): the phenyl fragments are turned in the same direction;
- model 5 ( $C_s$  symmetry): the phenyl fragments are turned in the opposite direction.

All quantum-chemical calculations predict almost identical geometrical parameters for models 1–5, except those torsion angles defining the orientation of the phenylethynyl fragments: the bond lengths differ by less than 0.005 Å and valence angles differ by less than 0.1° in the rings and by less than 6° in the alkyne chain. This indicates that the orientation of the phenylethynyl fragments relative to each other in 1,8-BPEA has a minor to negligible influence on the structural parameters of the different molecular models. The use of DFT functionals CAM-B3LYP, LC-BLYP taking into account long-range corrections effects for optimization of 1,8-BPEA led to similar values of angles on the one hand, and a shortening of the C–C distances within the rings on the other hand as compared with B3LYP/cc-pVTZ.

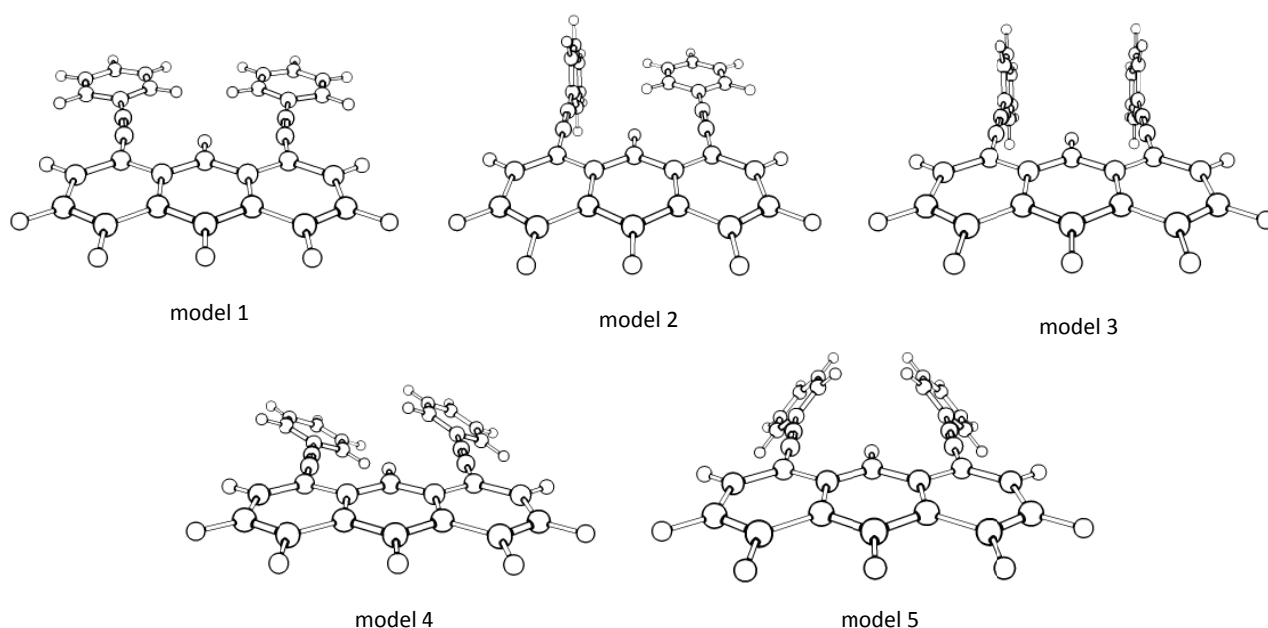


Fig. 1 Structural models for 1,8-bis(phenylethynyl)anthracene (**1**).

**Table 1** Relative energies (kcal/mol) and number of imaginary frequencies (NIF) predicted by calculations at different theory levels for models 1–5

	model 1	model 2	model 3	model 4	model 5
<b>B3LYP/cc-pVTZ</b>					
$\Delta E$	– <sup>a</sup>	0.5	1.9	0.0	1.1
NIF	–	1	2	0	1
<b>CAM-B3LYP/cc-pVTZ</b>					
$\Delta E$	1.7	0.2	1.7	0.0	1.2
NIF	2	1	2	0	1
<b>LC-BLYP/cc-pVTZ</b>					
$\Delta E$	2.3	0.0	1.9	0.05	1.4
NIF	2	–	2	0	1
<b>B3LYP-D2/cc-pVTZ</b>					
$\Delta E$	2.6	0.0	2.8	0.1	2.0
NIF	2	1	2	1	– <sup>b</sup>
<b>B3LYP-D3/cc-pVTZ</b>					
$\Delta E$	2.7	0.1	2.4	0.0	2.1
NIF	2	1	1	0	1

<sup>a</sup> The optimization process did not converge in the case of model 1.

<sup>b</sup> Calculation of frequencies failed.

On the contrary, the geometry parameters calculated with functionals taking explicitly into account the dispersive interaction, B3LYP-D2/cc-pVTZ and B3LYP-D3/cc-pVTZ, are very close to those at B3LYP/cc-pVTZ level of theory except the valence angles of the linear chain  $-C\equiv C-C-$  and the distances between phenylethynyl groups. Structural parameters obtained with use of LC-BLYP, LC-wPBE and M06 methods are given in Table S1 (S.I.).

The main problem of the calculations is the reliability of prediction of the conformer of minimum electronic energy (Table 1). None of the methods used predicted the main conformer without doubt concerning the typical error ranges of these methods. However, model 4 seems to be more realistic for a free molecule of 1,8-BPEA considering the interaction between the two phenyl rings. For this reason both, model 2 and 4, both corresponds to minima on the PES in some calculations, were tested in GED structural analysis.

### Experimental gas phase structure

The structural analysis of 1,8-BPEA presents a difficult problem. The bonded distances were determined with the typical precision of a GED study. The parameters describing the positions of phenylethynyl substituents relative to the anthracene fragment were also determined. However, a reliable determination of the parameters corresponding to phenyl-phenyl distances from GED data is difficult because the vibrational analysis, typically undertaken by the program SHRINK,<sup>27</sup> predicts enormous root mean square amplitudes of vibration  $I_{ij}$  and vibrational corrections  $\Delta r = r_a - r_{h1}$  for some atom pairs. It has become usual in the analysis of intensities of scattered electrons (GED) to include such vibrational information derived from quantum-chemical calculations (or experiments) to facilitate least-squares refinement by providing realistic starting values of vibrational amplitudes and by constraining groups of internuclear distances to reduce the correlation problem. For this purpose root-mean-square vibrational amplitudes  $I_{ij}$  and vibrational corrections  $\Delta r$  have in many GED studies been calculated and using either rectilinear or curvilinear relations between Cartesian and internal coordinates.<sup>27,28</sup> The curvilinear approach is generally considered to be more realistic and physically appealing. The program SHRINK<sup>27</sup> has frequently been successfully applied in this context. However, in the present case of 1,8-BPEA, a molecule with linear chains  $C-C\equiv C-C$ , the

use of the rectilinear or the curvilinear approximations led to unreasonably large vibrational corrections and root-mean-square vibrational amplitudes associated with internuclear distances that determine the relative positions of the phenylethynyl groups. Therefore we decided to use a novel method of calculating vibrational amplitudes and corrections utilizing molecular dynamics (MD) simulations.<sup>29</sup>

It should first be mentioned that many vibrational amplitudes related to phenyl-phenyl distances in 1,8-BPEA have values of about 1 Å; this means that the contribution of these distances to the molecular scattering intensity  $sM(s)$  curve is not very significant. To test this further, a least-squares analysis was carried out without taking these terms into account; this led to a value of  $R_f$  higher than optimal by only 0.06%. Nevertheless, we are confident that the relative positions of the phenyl groups were reliably determined because distances between atoms of the phenyl fragment and those of the anthracene skeleton are associated with much smaller vibrational amplitudes.

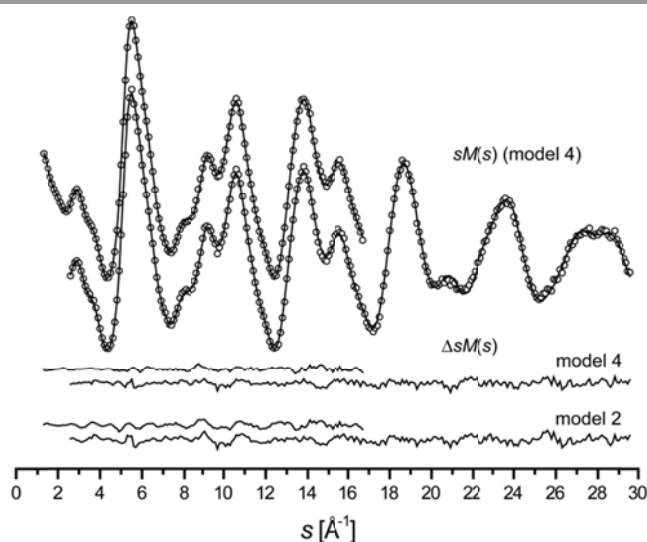


**Fig. 2** Experimental (dots) and theoretical (line) molecular scattering intensities  $sM(s)$  and their difference  $\Delta sM(s)$  for model 2 and model 4. The theoretical molecular intensity  $sM(s)$  is shown for model 4.

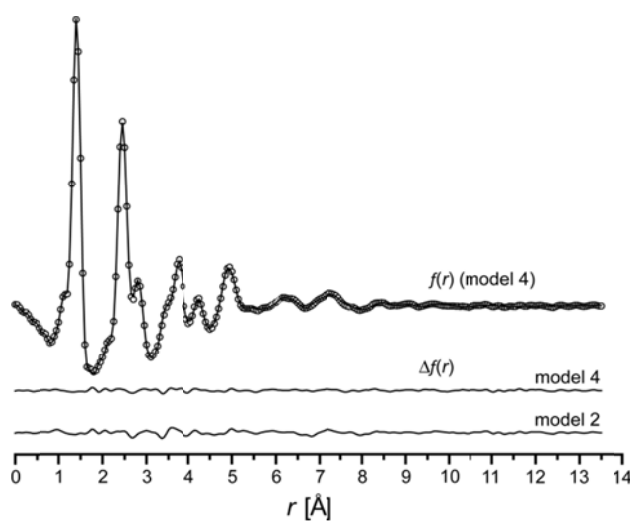


**Fig. 3** Experimental (dots) and theoretical (line) radial distribution curves  $f(r)$  and their differences  $\Delta f(r)$  for model 2 and model 4. The theoretical  $f(r)$  is shown for model 4.

The disagreement factor  $R_f$  between theoretical and experimental  $sM(s)$  functions for model 2 exceeds the one for model 4 by 1.1%. Therefore, and according to Hamilton's criterion,<sup>30</sup> model 2 had to be rejected at the 0.05 significance level. For this reason, the results of structural refinement of only model 4 are presented in Table S1 (Supplementary Information, S.I.). For this model, the disagreement factor  $R_f$  is 4.3%. The success of the refinement can be seen comparing the experimental molecular scattering intensities  $sM(s)$  and the radial distribution curves and their difference curves to the model curves as shown in Fig. 2 and 3, respectively.

It should be noted, the results of the GED study are in appropriate agreement with the structure of  $C_2$  symmetry predicted by B3LYP/cc-pVTZ level of theory.

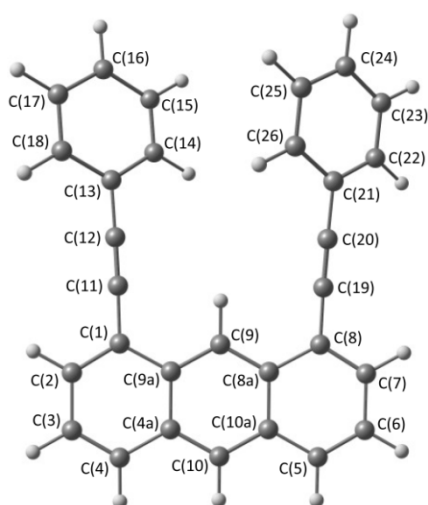


Fig. 4 Molecular structure and atom numbering of 1,8-BPEA ( $C_2$  symmetry).

However, the C–C distances in the ring system and the triple bond ( $C\equiv C$ ) calculated by DFT methods including long-range or dispersion corrections (CAM-B3LYP, LC-BLYP, LC-wPBE) and dispersive interaction (B3LYP-D2 and B3LYP-D3) are shorter than the experimental values. The distance between the centers of the phenyl rings in the experimental structure  $r(\text{Ph-Ph}) = 4.9 \text{ \AA}$  is about by  $1 \text{ \AA}$  shorter than that calculated at B3LYP/cc-pVTZ level of theory ( $6.0 \text{ \AA}$ ). However, taking into account dispersive interactions by using B3LYP-D2/cc-pVTZ and B3LYP-D3/cc-pVTZ approximations lead to the values of  $r(\text{Ph-Ph}) = 5.3$  and  $5.2 \text{ \AA}$ , respectively.

The vibrational amplitudes refined from GED intensities in this work significantly exceed the amplitudes calculated by the MD approach. In spite of this fact, the experimental vibrational amplitudes seem to be quite reliable because they are very close to values usually found for C–C and C–H distances (Table S2, S.I.). They are, for example, in excellent agreement with the corresponding calculated vibrational amplitudes of unsubstituted anthracene.

### Solid state structure

The molecular structure of 1,8-BPEA does not change noticeably concerning bond lengths and angles of directly bonded atoms when moving from gas phase to solid state, but the conformation changes substantially. The ideal  $C_2$  symmetry observed in the gas phase vanishes and a large variability of conformers is observed resulting from a complex pattern of intermolecular interactions.

1,8-BPEA crystallizes in the monoclinic space group  $P2_1/n$  with 14 molecules per unit cell, 3.5 molecules per asymmetric unit. Three independent molecules exhibit full site occupancy; a fourth one is disordered about an inversion center possessing a site occupancy factor of 0.5.

Table 2 Selected bond lengths [ $\text{\AA}$ ] and angles [ $^\circ$ ] of the 1,8-BPEA molecule determined by quantum-chemical calculations (single molecule), X-ray diffraction (XRD, single crystal)<sup>a</sup> and gas-electron diffraction (GED) experiments. See Table S2 (S.I.) for more data

	DFT/cc-pVTZ, $r_e$			XRD <sup>a,b</sup>		GED <sup>b</sup>
	B3LYP	CAM-B3LYP	B3LYP-D3	minimum	maximum	$r_e$
C(1)–C(2)	1.379	1.366	1.378	1.369(2)	1.375(2)	1.378(6)
C(1)–C(9a)	1.444	1.440	1.444	1.439(2)	1.445(2)	1.443(6)
C(1)–C(11) <sup>c</sup>	1.419	1.424	1.418	1.426(2)	1.432(2)	1.422(7)
C(4)–C(4a)	1.423	1.423	1.424	1.421(2)	1.428(2)	1.422(6)
C(9)–H <sup>c</sup>	1.080	1.080	1.080	–	–	1.085(5)
C(10)–C(4a) <sup>c</sup>	1.394	1.388	1.394	1.390(2)	1.396(2)	1.393(6)
C(11)–C(12) <sup>c</sup>	1.209	1.200	1.208	1.201(2)	1.203(2)	1.205(8)
C(12)–C(13)	1.422	1.426	1.420	1.428(2)	1.432(2)	1.424(7)
C(13)–C(18) <sup>c</sup>	1.404	1.395	1.404	1.386(2)	1.400(2)	1.411(6)
av. C(Ant)–C(Ant) <sup>d</sup>	1.410	1.403	1.406	1.403(2)	1.403(2)	1.409(6)
C(1)–C(11)–C(12)	177.5	178.1	178.2	173.1(1)	179.2(1)	179.8(33)
C(4a)–C(10)–C(10a) <sup>c</sup>	122.0	121.9	122.0	121.5(1)	122.0(1)	121.8(7)
C(9a)–C(4a)–C(4) <sup>c</sup>	119.4	119.4	119.2	119.4(1)	119.5(1)	119.2(4)
C(9a)–C(4a)–C(4) <sup>c</sup>	119.4	119.4	119.2	119.4(1)	119.5(1)	119.2(4)
C(11)–C(12)–C(13)	178.9	179.2	179.3	175.1(1)	179.1(1)	178.9(33)
C(12)–C(13)–C(18) <sup>c</sup>	120.5	120.4	120.8	119.7(1)	121.5(1)	120.4(13)
$r[\text{C(18)–C(13)–C(1)–C(2)}]^f$	22.7	25.4	25.1	7.1(1)	37.6(1)	24.4(180)

<sup>a</sup> Only the non-disordered molecules (molecules 1–3) are taken into account.

<sup>b</sup> Experimental errors are given as  $1\sigma$  for XRD and as  $\sigma = [(0.002r)^2 + (2.5\sigma_{15})^2]^{1/2}$  for distances and  $\sigma = 3\sigma_{15}$  for angles for GED.

<sup>c</sup> Independent parameters.

<sup>d</sup> Average C–C distances in the anthracene fragment (XRD: range).

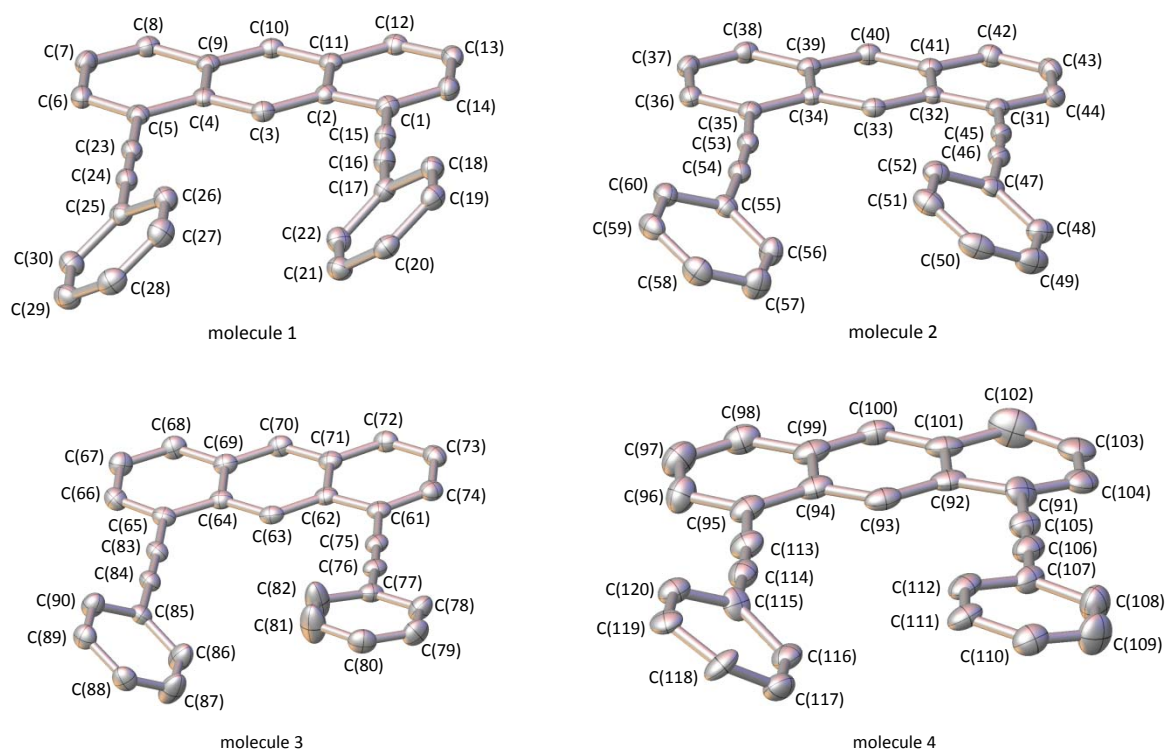


Fig. 5 Crystal structure of 1,8-BPEA as thermal ellipsoid plots with numbering scheme of the four independent molecules. Hydrogen atoms are omitted for clarity; thermal ellipsoids are drawn at 50% probability level.

None of the four molecules shows  $C_2$  symmetry (Fig. 5). Selected bond lengths and angles of 1,8-BPEA are listed in Table 2. In fact, the anthracene units show only small differences, overlaying these pairwise (while neglecting the hydrogen atoms) the root-mean-square deviation (RMSD) is not higher than 0.047 Å. Due to the flexibility of the phenylethynyl groups, the RMSD for the complete molecules increases to values between 0.16 Å and 0.33 Å (Fig. 6). As shown in an image of an overlay of all four molecules (Fig. 6b), the torsion of the phenyl groups shows a wide variability. The dihedral angles of these rings to the corresponding outer ring of the anthracene unit is in the range between 6.0(2)° and 37.4(1)°, the dihedral angles between the two phenyl groups inside one molecule is in the range between 0.9(1)° and 30.7(1)°. Despite of this large variance of dihedral angles, the distances between the *ortho*-carbon atoms of two phenyl groups facing each other within one molecule are all in the range from 3.50(1) to 3.67(1) Å, correspondingly the *meta*-carbon atoms show distances between 3.61(1) and 3.83(1) Å. In each molecule, the distance between the *meta*-carbon atoms is larger than that between the *ortho*-carbon atoms. None of the eight alkyne bonds C–C≡C–C shows ideal linearity; the angles enclosed by the center of the triple bond and the two aromatic carbon atoms it is bonded to are in the range of 178.9(1)° to 173.0(1)°. The occurrence of steric stress can also be estimated from the angles of the carbon atoms in position 1 and 8 (*ipso*-carbon atoms) of the anthracene unit to the *ipso*-

carbon atoms of the phenyl groups; this is expected to be orthogonal, but measures in a range between 86.2(1)° to 99.1(1)°.

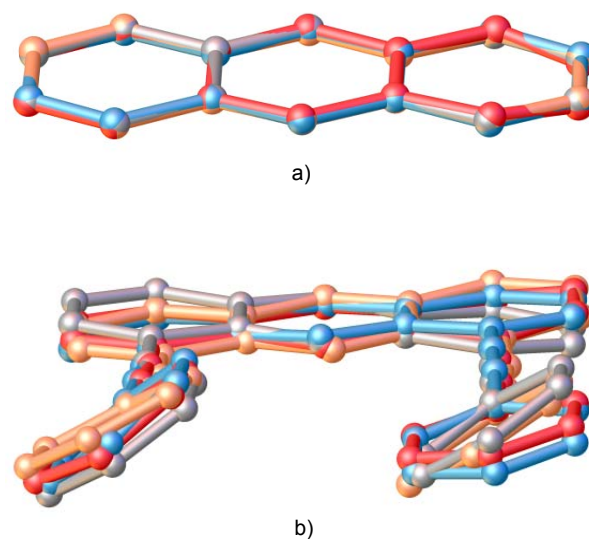


Fig. 6 Overlay of the four independent molecules of 1,8-BPEA (1) with minimized RMSD for a) anthracene units and b) all carbon atoms. Grey: molecule 1 [C(1)–C(30)], orange: molecule 2 [C(31)–C(60)], blue: molecule 3 [C(61)–C(90)], red: molecule 4 [C(91)–C(120)].

However, the sum of two of these angles within one molecule varies in a narrow range from 184.3° to 185.4°. As this is above the ideal 180° it might indicate repulsion between the phenyl groups within one molecule, which is supported by the fact of larger distances between pairs of *meta*- than between pairs of *ortho*-carbon atoms.

None of the eight alkyne bonds C–C≡C–C shows ideal linearity; the angles enclosed by the center of the triple bond and the two aromatic carbon atoms it is bonded to are in the range of 178.9(1)° to 173.0(1)°. The occurrence of steric stress can also be estimated from the angles of the carbon atoms in position 1 and 8 (*ipso*-carbon atoms) of the anthracene unit to the *ipso*-carbon atoms of the phenyl groups; this is expected to be orthogonal, but measures in a range between 86.2(1)° to 99.1(1)°.

The crystal structure is shown in Fig. 7 and can be described as a herringbone pattern by established by packing of trimeric and dimeric piles of molecules. The intermolecular forces can be classified as  $\sigma\cdots\pi$  as well as  $\pi\cdots\pi$  interactions (Table 4). The  $\pi\cdots\pi$  bonds were defined for aromatic rings with distances between their centroids smaller than 4 Å. There are two types of  $\pi\cdots\pi$  interactions: two independent molecules (molecules 1 and 2) are forming a head to head orientated dimer by  $\pi\cdots\pi$  interactions between their anthracene units [3.76(1) and 3.78(1) Å], but they do not show  $\pi\cdots\pi$  bonds involving their phenyl groups (Fig. 8a). A trimer is formed by interactions between molecule 3 and its symmetry equivalent with a third molecule (molecule 4) disordered about a center of inversion located in the middle of the trimer (Fig. 8c). The outer molecules are orientated head to tail with respect to each other; this leads to one head-to-head as well as one head-to-tail orientation within this trimeric unit.

The  $\pi\cdots\pi$  interaction between the anthracene units of the head-to-head neighbors measures 3.65(1) Å. The head-to-tail oriented neighbors show  $\pi\cdots\pi$  interactions between the phenyl units of the outer and the anthracene units of the central molecule; the associated distances are 3.78(1) and 3.97(1) Å (Fig. 8c). There are exactly these two phenyl groups that show the remarkably small dihedral angles to their anthracene units [6.0(1)° and 13.2(1)°], so it is obvious that these intermolecular dispersive  $\pi\cdots\pi$  interactions change the molecular geometry with respect to the free molecule. Furthermore, the shortest distance between *ortho*-phenyl carbon atoms of 3.50(1) Å corresponds to the smallest dihedral angle of 6.0(2)° (Fig. 8b, Table 3).

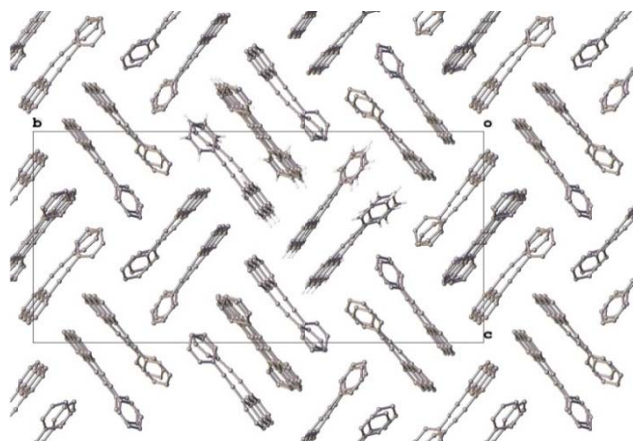


Fig. 7 Crystal structure of 1,8-BPEA (1) in a view along the *a* axis.

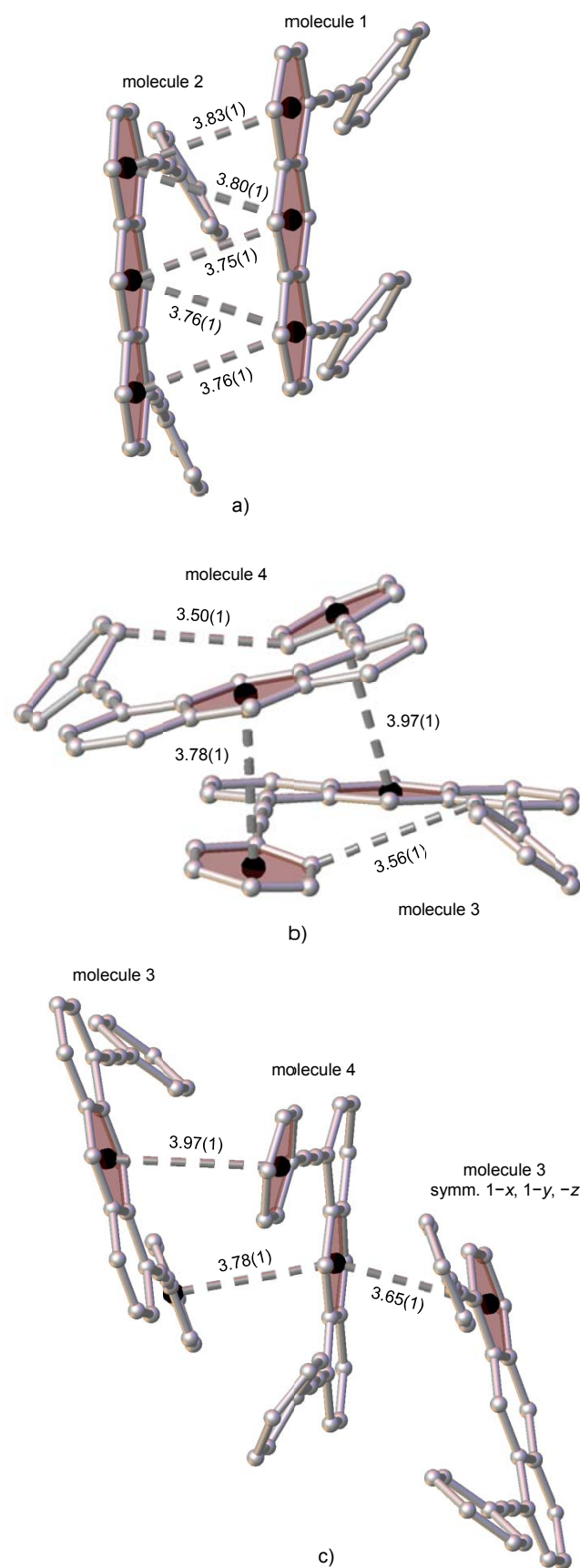


Fig. 8 Intermolecular interactions in a) the head-to-head oriented dimer, b) the head-to-tail oriented neighbors inside the trimer and c) the trimer. Distances are given in Å.

**Table 3** Selected distances [Å] and angles [°] of the 1,8-BPEA molecules determined by XRD (solid state). Atom numbering see Fig. 5

	molecule 1	molecule 2	molecule 3	molecule 4
Dihedral angle anthracene/phenyl rings <sup>a</sup>	35.3(1) / 37.4(1)	28.3(1) / 26.6(1)	13.2(1) / 34.6(1)	6.0(2) / 32.9(2)
Dihedral angle phenyl rings/phenyl rings <sup>b</sup>	0.9(1)	5.9(1)	30.7(1)	22.3(2)
Dihedral angle outer anthracene rings <sup>c</sup>	3.6(1)	3.1(1)	2.3(1)	5.5(2)
Angle enclosed by center of triple bond to atoms bonded to C≡C <sup>d</sup>	178.0(1) / 178.9(1)	173.5(1) / 173.1(1)	173.5(1) / 178.4(1)	178.0(3) / 175.5(3)
Angle enclosed <i>ipso</i> -anthracene C atoms to <i>ipso</i> -phenyl C <sup>e</sup>	92.9(1) / 91.5(1)	86.2(1) / 99.1(1)	92.0(1) / 93.3(1)	89.6(2) / 95.4(2)
Distance between closest <i>ortho</i> -phenyl C atoms <sup>f</sup>	3.52(1)	3.68(1)	3.56(1)	3.50(1)
Distance between closest <i>meta</i> -phenyl C atoms <sup>g</sup>	3.61(1)	3.83(1)	3.74(1)	3.66(1)

<sup>a</sup> Plane C(1)–C(2)–C(11)–C(12)–C(13)–C(14) vs. C(17)–C(18)–C(19)–C(20)–C(21)–C(22) and plane C(4)–C(5)–C(6)–C(7)–C(8)–C(9) vs. C(25)–C(26)–C(27)–C(28)–C(29)–C(30).

<sup>b</sup> Plane C(17)–C(18)–C(19)–C(20)–C(21)–C(22) vs. C(25)–C(26)–C(27)–C(28)–C(29)–C(30).

<sup>c</sup> Plane C(1)–C(2)–C(11)–C(12)–C(13)–C(14) vs. C(4)–C(5)–C(6)–C(7)–C(8)–C(9).

<sup>d</sup> Angle C(1)–[center of C(15) and C(16)]–C(17) and angle C(5)–[center of C(23) and C(24)]–C(25).

<sup>e</sup> Angle C(5)–C(1)–C(17) and C(25)–C(5)–C(1).

<sup>f</sup> Distance C(22)–C(26).

<sup>g</sup> Distance C(21)–C(27).

For molecules 2, 3 and 4 the atom numbering is  $n+30$ ,  $n+60$  and  $n+90$ , respectively.

No  $\pi\cdots\pi$  interactions were found between the dimeric and trimeric molecular units, however, contacts of the  $\sigma\cdots\pi$  type are linking these units (Table 4). The shortest  $\sigma\cdots\pi$  contact is found to be 2.57(1) Å between an anthracene hydrogen [at C(40)] and an alkyne carbon atom, accompanied by a distance to the second alkyne carbon atom at 2.71(1) Å. In addition, six intermolecular hydrogen-carbon contacts smaller than 2.8 Å were found, all involving phenyl carbon atoms (Fig. 9).

The variability of structural parameters of independent molecules for the same compound is also observable in the XRD results of 1,8-diethynylantracene<sup>10</sup> or 1,8-bis[(trimethylsilyl)ethynyl]- and 1,8-bis[(trimethylstannyl)ethynyl]anthracene, respectively.<sup>8</sup>

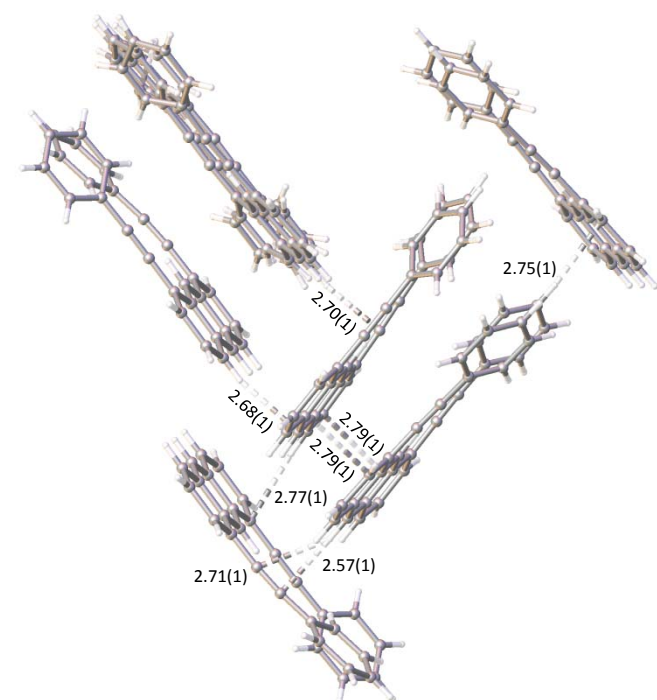


**Fig. 9** Intermolecular contacts between dimers and trimers with intermolecular hydrogen carbon contacts smaller than 2.8 Å. No further  $\sigma\cdots\pi$  contacts are found.

**Table 4** Selected intermolecular distances of the 1,8-BPEA molecules determined by XRD (solid state). Atom numbering see Fig. 5. Hydrogen numbering corresponds to C numbering

	$\pi\cdots\pi$ contacts		$\sigma\cdots\pi$ contacts
head-to-head dimer	3.78(1) / 3.76(1) <sup>a</sup>	H(12)⋯C(65) <sup>d</sup>	2.77(1)
head-to-head trimer	3.65(1) <sup>b</sup>	H(13)⋯C(36) <sup>e</sup>	2.79(1)
head-to-tail trimer	3.78(1) / 3.96(1) <sup>c</sup>	H(36)⋯C(13) <sup>f</sup>	2.79(1)
		H(40)⋯C(76) <sup>g</sup>	2.57(1)
		H(40)⋯C(75) <sup>g</sup>	2.71(1)
		H(50)⋯C(36) <sup>h</sup>	2.75(1)
		H(68)⋯C(10) <sup>f</sup>	2.68(1)

<sup>a</sup> Centroid distance [C(4)–C(5)–C(6)–C(7)–C(8)–C(9)] to [C(32)–C(33)–C(34)–C(39)–C(40)–C(41)] and centroid distance [C(2)–C(3)–C(4)–C(9)–C(10)–C(11)] to [C(31)–C(32)–C(41)–C(42)–C(43)–C(44)].

<sup>b</sup> Centroid distance [C(61)–C(62)–C(71)–C(72)–C(73)–C(74)] generated by symmetry  $1-x, 1-y, -z$  to [C(92)–C(93)–C(94)–C(99)–C(100)–C(101)].

<sup>c</sup> Centroid distance [C(77)–C(82)] to [C(92)–C(93)–C(94)–C(99)–C(100)–C(101)] and centroid distance [C(62)–C(63)–C(64)–C(69)–C(70)–C(71)] to [C(107)–C(102)].

<sup>d</sup> Carbon atom generated by symmetry  $1-x, 1-y, 1-z$ .

<sup>e</sup> Carbon atom generated by symmetry  $x-1, y, z$ .

<sup>f</sup> Carbon atom generated by symmetry  $x+1, y, z$ .

<sup>g</sup> Carbon atom generated by symmetry  $1-x, 1-y, 1-z$ .

<sup>h</sup> Carbon atom generated by symmetry  $x - \frac{1}{2}, \frac{1}{2} + y, z - \frac{1}{2}$ .

### Orientation preference of the phenyl fragments – role of $\pi$ -electron delocalization

According to DFT calculations and GED experiments, the main structural feature of 1,8-BPEA is the co-directional rotation of the phenylethynyl fragments (the dihedral angles are 24° in the gas phase (GED)). The four molecules in the solid state show a distribution of such angles between 0.9° and 30.7°, but as mentioned above, the small values are associated with phenyl groups involved in significant intermolecular interactions. The situation observed for the free molecule is thus reflected in most but these molecules in the crystal and the variations obviously depend on weaker inter- and intramolecular interactions.

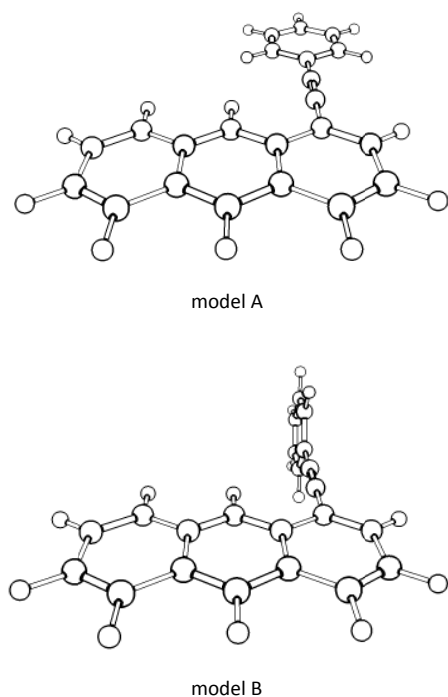


Fig. 10 Structural models for 1-(phenylethynyl)anthracene (1-PEA).

In order to shed more light on the reason for the co-directional rotation of the phenylethynyl fragments in 1,8-BPEA, we studied first a simplified case with one substituent only: 1-(phenylethynyl)anthracene (1-PEA). We calculated two conformations with coplanar and perpendicular orientation of the phenyl plane versus the anthracene system (Fig. 10). According to the calculations, the coplanar conformer (model A) corresponds to a minimum on the potential energy surface, whereas the perpendicular one (model B) represents a maximum in energy. This is because in the case of model A,  $\pi$ -delocalization is spread over the whole carbon skeleton, whereas in model B the  $\pi$ -electron system is divided into separate parts (Ph–C $\equiv$ C– and –C $\equiv$ C–anthracene). The total energy of donor-acceptor interaction between the orbitals of the triple bond C $\equiv$ C (components  $\sigma$ ,  $\pi_1$  and  $\pi_2$ ) and the  $\sigma$  and  $\pi$ -orbitals of phenyl and anthracene fragments is 109.2 kcal/mol for model A and 104.6 kcal/mol for model B.

For 1,8-BPEA, the coplanar position of the phenylethynyl groups to the anthracene plane (model 1, Fig. 1) is energetically unfavorable due to mutual repulsion of the phenyl fragments, i.e. too close H...H contacts.

In the case of model 3 with both phenylethynyl fragments oriented perpendicular to the anthracene plane, steric strain between the neighboring groups would be minimal, but this form is energetically unfavorable due to minimized  $\pi$ -electron delocalization as was shown for model B of 1-PEA. On the contrary, structures 2 and 4 represent a balance between extended  $\pi$ -electron delocalization of the phenylethynyl and anthracene fragments and low steric repulsion of the phenyl groups.

As mentioned above, the GED results show that model 2 can be rejected. Thus, model 4 with the co-directional rotated phenylethynyl fragments is the most preferable for the 1,8-BPEA molecule among the five models under investigation (Fig. 1).

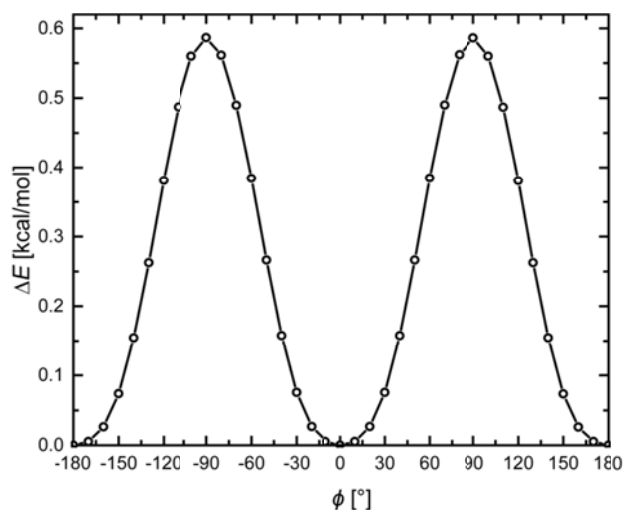


Fig. 11 Potential function for internal rotation of the phenylethynyl group of 1-(phenylethynyl)anthracene (1-PEA).

Fig. 11 shows the potential function concerning the internal rotation of the phenylethynyl group for the mono-substituted anthracene. It has to be noted that in contrast to double bonds, the rotation about single and triple bond containing –C $\equiv$ C– units is virtually free as far as the electronic structure is concerned; the barrier to internal rotation of about 0.6 kcal/mol is mainly due to repulsion between hydrogen atoms at position 9 of the anthracene and the correspondingly facing *ortho*-phenyl position.

The potential function for internal rotation (Fig. 11) shows that it costs little energy to turn the phenylethynyl group by 25.4° as it is found in the optimized structure of model 4 for 1,8-BPEA (Fig. 1). According to the NBO analysis, the totally delocalized  $\pi$ -electron system is not interrupted to a large extent in the case of co-directional rotation of the phenylethynyl fragments to such comparably small dihedral angles (Fig. 1, model 4), and the sum of the energies of donor-acceptor interaction between the orbitals of the triple –C $\equiv$ C– bond and the  $\sigma$  and  $\pi$  orbitals of the one phenyl and anthracene fragments is about 107 kcal/mol; this is somewhat less than in model A (109.2 kcal/mol).

It is important that the steric repulsion in model 4 decreases considerably as compared with that in model 1: the shortest H...H distances between two phenyl fragments changes from 2.1 Å to 2.8 Å. The last value exceeds significantly the sum of van der Waals-radii of two hydrogen atoms (2.4 Å).<sup>31</sup>

The lengths of the linear chain ( $C_{\text{Ant/Ph}}-C_{\text{Ph}}$ ) in models 1 and 4 of 1,8-BPEA (Fig. 1) and the planar models of diphenylethyne (DPE) and 1-PEA are very close while the chains in the model 3 of 1,8-BPEA and perpendicular models of DPE and 1-PEA are about 0.006 Å longer. Elongation of the chain in the case of model 3 is caused by weakening the  $\pi$ -electronic delocalization as compared with models 1 and 4. The rotational barrier of DPE calculated at CAM-B3LYP/cc-pVTZ level of theory (2.7 kJ/mol) is close to the barrier of 1-PEA (2.5 kJ/mol), and it is in a good agreement with the results of previous calculations at B3LYP/6-311+G\*\* approximation.<sup>32</sup> In the case of 1,8-BPEA, the rotation of the phenyl groups leading to planar (model 1) and perpendicular (model 3) configurations is restricted and it appears in the values of  $\Delta E$  (see Table 1) required for this movement: these values are about 3.5 times higher than that for DPE and 1-PEA molecules.

**Table 5** HOMO and LUMO energies for the optimized structures of 1,8-bis(phenylethynyl)anthracene (1, 1,8-BPEA) and the 1-(phenylethynyl)anthracene (1-PEA)

	1,8-BPEA (model 4)	1-PEA (model A)	1-PEA (model B)
$E(\text{HOMO})$ , eV	-6.609	-6.655	-6.728
$E(\text{LUMO})$ , eV	-1.200	-1.060	-0.949
$\Delta E_{(\text{LUMO-HOMO})}$ , eV	5.409	5.595	5.779

The energies of the canonical frontier MOs are presented in Table 5. The energies of HOMO and LUMO show that the energy gap decreases in 1,8-BPEA with respect to 1-PEA. It is known, that the extension of the  $\pi$ -electronic system increases the HOMO energy and decreases the LUMO energy; our calculations confirm this statement.

A related molecule with two phenylethynyl groups occupying the positions at C(9) and C(10) of anthracene (9,10-BPEA) has been studied earlier by X-ray crystallography.<sup>33</sup> In 9,10-BPEA the central anthracene fragment and the two phenylethynyl groups have been found to be nearly coplanar. This means that under the absence of steric repulsion between neighboring phenyl groups the molecule adopts a planar structure (dispersive-type  $\pi$ -stacking forces in the crystalline phase do not alter the molecular structure in this case). In case of 1,8-BPEA the molecule avoids a planar structure due to steric repulsion between the phenylethynyl substituents. The deviations between solid state and gas phase and the occurrence of four differently twisted forms in the same crystal confirms the flatness of the torsion potential and shows how dispersive-type  $\pi$ -stacking forces may alter a structure in this phase.

#### Orientation preference of the phenyl fragments – role of dispersion interactions

Another possible factor that might play a significant role in determining the relative orientation of the phenylethynyl groups in 1,8-BPEA are dispersion interactions between them. In order to estimate the energy of possible dispersive attractions between two phenylethynyl groups  $E_{\text{disp}}(\text{PhCC-PhCC})$  for models 1–5, B3LYP-D2/cc-pVTZ calculations were carried out (Table 6). The value of the Grimme-D2 dispersion energy  $E_{\text{disp}}(\text{PhCC-PhCC})$  was estimated by this definition:

$$E_{\text{disp}}(\text{PhCC-PhCC}) = E_{\text{disp}}(\text{C}_{30}\text{H}_{18}) - 2E_{\text{disp}}(\text{PhCC-Ant}) - 2E_{\text{disp}}(\text{C}_6\text{H}_6) - E_{\text{disp}}(\text{Ant}),$$

with  $E_{\text{disp}}(\text{PhCC-Ant})$  being the energy of the dispersion interaction between phenylethynyl group and anthracene fragment,  $E_{\text{disp}}(\text{C}_{30}\text{H}_{18})$  being the total dispersion energy of 1,8-BPEA,  $E_{\text{disp}}(\text{C}_6\text{H}_6)$  the dispersion energy of benzene, and  $E_{\text{disp}}(\text{Ant})$  the dispersion energy of anthracene. The  $E_{\text{disp}}(\text{PhCC-Ant})$  component was calculated as follows:

$$E_{\text{disp}}(\text{PhCC-Ant}) = E_{\text{disp}}(\text{C}_{22}\text{H}_{14}) - E_{\text{disp}}(\text{C}_6\text{H}_6) - E_{\text{disp}}(\text{Ant}),$$

where  $E_{\text{disp}}(\text{C}_{22}\text{H}_{14})$  is the dispersion energy of 1-PEA.

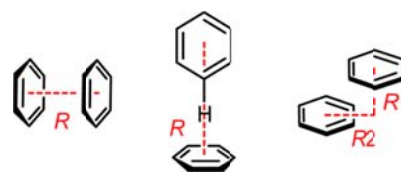
Grimme-D2 intramolecular dispersion energies of 1-(phenylethynyl)anthracene [ $E_{\text{disp}}(\text{C}_{22}\text{H}_{14})$ ], anthracene [ $E_{\text{disp}}(\text{Ant})$ ] and benzene [ $E_{\text{disp}}(\text{C}_6\text{H}_6)$ ] were determined from single point calculations which were performed using the atom coordinates obtained from the optimized geometries for each model of 1,8-

BPEA. It should be mentioned that the results of the B3LYP-D3/cc-pVTZ calculations could not be applied because the dispersion energy in this approximation contains non-additive three-body energy terms  $E(3)$ .<sup>23</sup>

Table 6 Total energies of dispersive interactions  $E_{\text{disp}}(\text{C}_{30}\text{H}_{18})$ , energies of the dispersive interaction of phenylethynyl fragments, and linear chain angles according to the calculations (see Fig. 4 for atom numbering)

energies [kcal/mol], angles [°]	model 1	model 2	model 3	model 4	model 5
<b>B3LYP-D2</b>					
$E_{\text{disp}}(\text{C}_{30}\text{H}_{18})$	-34.7	-38.3	-37.1	-36.8	-35.8
$E_{\text{disp}}(\text{PhCC-PhCC})$	-6.4	-9.6	-8.5	-8.3	-7.4
<b>B3LYP-D3</b>					
$E_{\text{disp}}(\text{C}_{30}\text{H}_{18})$	-25.7	-28.2	-28.4	-27.8	-26.5
<b>B3LYP-D2</b>					
C(1)–C(11)–C(12)/ C(8)–C(19)–C(20)	175.2	178.8/ 174.6	174.5	178.7	179.1
C(11)–C(12)–C(13)/ C(19)–C(20)–C(21)	178.0	178.2/ 176.5	178.7	179.6	179.5
<b>B3LYP-D3</b>					
C(1)–C(11)–C(12)/ C(8)–C(19)–C(20)	175.3	179.8/ 177.0	174.9	178.2	179.5
C(11)–C(12)–C(13)/ C(19)–C(20)–C(21)	178.0	179.1/ 178.2	178.6	179.3	179.6
<b>B3LYP</b>					
C(1)–C(11)–C(12)/ C(8)–C(19)–C(20)	*	179.1/ 179.0	178.9	177.5	176.3
C(11)–C(12)–C(13)/ C(19)–C(20)–C(21)	*	179.7/ 179.5	179.5	178.9	178.2

\* no convergence.

**Fig. 12** Sandwich (S), T-shaped (T) and parallel-displaced (PD) configurations of the benzene dimer.<sup>21a</sup>**Table 7** Comparison of the inter-phenyl distances in the benzene dimer and 1,8-BPEA

	S / model 3	T / model 2	PD / model 4	
	R	R	R1	R2
Benzene dimer, CCSD(T)/ aug-cc-pVDZ <sup>21a</sup>	4.	5.1	3.6	1.8
1,8-BPEA (B3LYP-D2/cc-pVTZ)	4.0	4.8	2.7	4.6
1,8-BPEA (B3LYP-D3/cc-pVTZ)	4.0	5.0	3.0	4.3
1,8-BPEA (B3LYP/cc-pVTZ)	5.6	5.6	3.0	5.1

As one can see from Table 6, the strongest dispersive attraction between two phenylethynyl groups occurs in model 2, while models 3 and 4 are almost isoenergetic in this respect. It is important to note that the orientation of the phenyl rings in models 2, 3 and 4 corresponds to T-shape (T), sandwich (S) and parallel-displaced (PD) configurations of the benzene dimer, respectively. The values  $E_{\text{disp}}(\text{PhCC-PhCC})$  obtained in the present work are in agreement with reported dispersion energies of the benzene dimer (Fig. 12).<sup>12</sup> Obviously, in the benzene dimer, the energy of dispersive attraction depends on the intermonomer distance. In the case of 1,8-BPEA, the movement of the phenyl rings towards each other is restricted by the rigid anthracene skeleton. This movement leads to decrease of the

angles C(1)–C(11)–C(12) and C(11)–C(12)–C(13) in the pseudo-linear chain –C–C≡C–. Substantial bendings of this chain in B3LYP-D2/cc-pVTZ and B3LYP-D3/cc-pVTZ calculations as compared with B3LYP/cc-pVTZ (see Table 6) in models 2 and 3 are

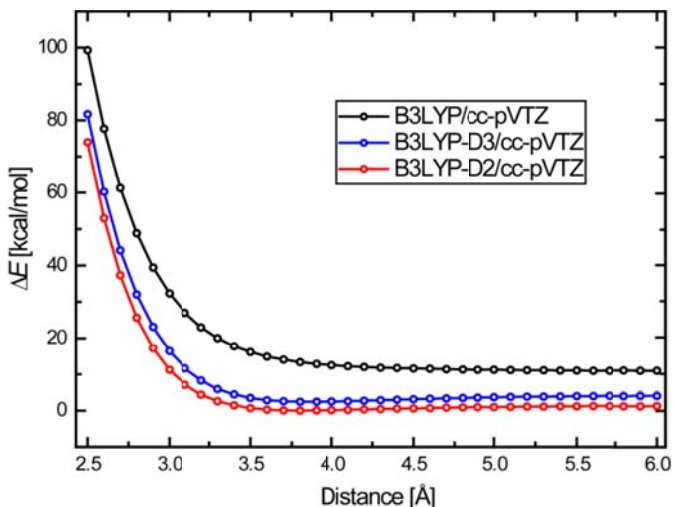


Fig. 13 B3LYP/cc-pVTZ (black), B3LYP-D2/cc-pVTZ (red) and B3LYP-D3/cc-pVTZ (blue) PECs for the S configuration of the benzene dimer.

apparently caused by dispersion forces. Both calculations, of models 4 and 5, show that the angles C(1)–C(11)–C(12) and C(11)–C(12)–C(13) are close to 180°. The bending of this pseudo-linear fragment by 4° was estimated to cost only about 0.3 kcal/mol in a B3LYP-D2/cc-pVTZ calculation for the model compound H<sub>3</sub>C–C≡C–CH<sub>3</sub>.

The interphenyl distances (see Fig. 12 for notation) in 1,8-BPEA predicted by B3LYP-D2/cc-pVTZ and B3LYP-D3/cc-pVTZ calculations, which take into account dispersion interactions, are significantly shorter than those obtained at the B3LYP/cc-pVTZ level. On the other hand, they happen to be surprisingly close to the intermonomer distances in the S and T configurations of the benzene dimer (see Table 7).

The potential energy curves (PECs) of interaction between benzene moieties in the S configuration of the benzene dimer were calculated utilizing B3LYP, B3LYP-D2 and B3LYP-D3 functionals combined with cc-pVTZ basis set. A plot of the PECs was implemented with a step of 0.1 Å along the line connecting the ring centers. The PECs calculated using the B3LYP-D functionals possess a minimum, while the B3LYP functional led to a monotonically decreasing curve (Fig. 13).

This confirms again that the pure B3LYP functional does not take into account dispersive interactions and the dispersion energy contribution is close to zero. We can see from Table 6 that Grimme dispersion energies calculated at the B3LYP-D3/cc-pVTZ level are maximal for models 2 and 3 and minimal for the planar model 1.

From the above discussion it becomes clear that the total values of dispersion energies are about four times lower than those of donor-acceptor interaction between the orbitals of the triple C(11)≡C(12) bond (components  $\sigma$ ,  $\pi_1$  and  $\pi_2$ ) and the  $\sigma$ - and  $\pi$ -orbitals of phenyl and anthracene fragments (see the previous section). Therefore, in the case of 1,8-BPEA dispersive attraction does not substantially affect the relative orientation of the phenyl groups plane to the plain of anthracene frag-

ment, but the attractive interaction shrinks the distance between the phenyl rings significantly.

Table 8 Comparison of structural parameters [Å/°] of 1,8-bis(phenylethynyl)anthracene (1,8-BPEA), anthracene and benzene calculated by B3LYP/cc-pVTZ

	1,8-BPEA	anthracene	benzene
$r[C(1)–C(9a)]$	1.444	1.425	
$r[C(1)–C(2)]$	1.379	1.363	
$r[C(13)–C(14)]$	1.403		1.391
$r[C(13)–C(18)]$	1.404		1.391
$\angle[C(2)–C(1)–C(9a)]$	119.5	121.0	
$\angle[C(18)–C(13)–C(14)]$	118.7		120.0

### Substitution effects in the phenyl and anthracene fragments

A comparison of the structures of anthracene and 1,8-BPEA molecules shows that the triple bond unit –C≡C– can be considered as a donor substituent with respect to both, the phenyl and anthracene fragments. Therefore, the bond lengths within the rings to the *ipso*-carbon atoms, i.e.  $r[C(13)–C(18)]$  and  $r[C(13)–C(14)]$  in the phenyl unit and  $r[C(9a)–C(1)]$  and  $r[C(1)–C(2)]$  in the anthracene fragments are found to be lengthened relative to native benzene or anthracene, respectively. In the same sense, the angles C(18)–C(13)–C(14) and C(2)–C(1)–C(9a) decrease (Fig. 4, Table 8).

### Conclusions

The structure of 1,8-bis(phenylethynyl)anthracene (1,8-BPEA) has been studied in both, gas phase and solid state, by a combined GED/MS method in synchronous mode and by XRD of a single crystal. In general, the experimental bond lengths are in appropriate agreement with those calculated by DFT methods. Concerning the conformations of 1,8-BPEA, different quantum-chemical methods, including such with corrections for dispersion interactions, give different result. According to joint GED and calculated data, a free molecule 1,8-BPEA adopts C<sub>2</sub> symmetry in its ground state with co-directionally rotated phenylethynyl groups, whereas other (phenylethynyl)anthracenes are of overall planar structure. The reason for the deviation from a planar structure in 1,8-BPEA is the result of a compromise between the loss of extended  $\pi$ -electron delocalization between the phenylethynyl and anthracene fragments and the optimization of steric repulsion between the phenyl substituents, that experience weak attraction by dispersive forces at the same time. However, these dispersive interactions do apparently not play the key role in determining the relative orientation of the phenyl groups but affect the distance between them. Such a physical picture may be used to explain the conformations of  $\pi$ -conjugated systems with aromatic substituents.

In the crystalline state, the four independent molecules deviate more or less from this ideal C<sub>2</sub> symmetry of the free molecule. They pack in piles of dimers and trimers held together predominantly by dispersive type  $\pi$ -stacking forces between the anthracene units (dimer and trimers) and the phenyl groups (trimers). The maximum variation of the molecular structure of 1,8-BPEA within the crystal relative to that of

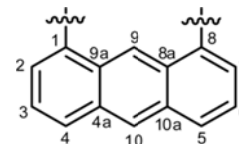
a free molecule is found within the trimeric piles, where the phenyl groups interact with the anthracene unit of a neighboring molecule; this has a pronounced effect on the conformation described by the dihedral angle between phenyl and anthracene units within the molecule. The possibility to change this conformation is due to the relatively flat potential of torsion, the result of mutually antagonizing effects of extended  $\pi$ -conjugation and mutual repulsion of the phenyl groups. The molecular dimeric and trimeric piles are found to be packed in a herringbone arrangement, linked by intermolecular  $\sigma(\text{CH})\cdots\pi$  interactions.

## Experimental

### Synthesis

**General Remarks.** Synthesis of 1,8-dichloroanthracene is described elsewhere.<sup>24</sup> The reaction was carried out under an anhydrous, inert atmosphere of nitrogen using standard Schlenk techniques in dry THF (dried over potassium and freshly distilled before being used for the reactions). Column chromatography was performed on silica gel 60 (0.04–0.063 mm mesh). NMR spectra were recorded on a Bruker *DRX 500* and a Bruker *Avance III 500* instrument at ambient temperature; the chemical shifts ( $\delta$ ) were measured in ppm with respect to the solvent ( $\text{CDCl}_3$ :  $^1\text{H}$  NMR  $\delta = 7.26$  ppm,  $^{13}\text{C}\{^1\text{H}\}$  NMR  $\delta = 77.16$  ppm). EI mass spectra were recorded using an *AutospecX* magnetic sector mass spectrometer with EBE geometry (Vacuum Generators, Manchester, UK) equipped with a standard EI source. Samples were introduced by a push rod in aluminum crucibles. Ions were accelerated by 8 kV. The numbering scheme for NMR assignments (Scheme 2) is based on IUPAC guidelines.

**1,8-Bis(phenylethynyl)anthracene.** Phenylacetylene (5.0 mL, 47.7 mmol) was added dropwise to a solution of ethylmagnesium bromide (1 M in THF) at 0 °C. The mixture was stirred at room temperature for 2 h and gas evolution was observed. The formed phenylethynylmagnesium bromide was slowly added to a solution of dichloroanthracene (1.20 g, 4.9 mmol),  $\text{Ni}(\text{acac})_2$  (6 mg, 0.023 mmol) and  $\text{PPh}_3$  (10 mg, 0.038 mmol) in THF (50 mL) at room temperature, while the colour of the solution changed from yellow to dark red. The mixture was heated to reflux for 72 h and then quenched with a saturated aqueous solution of  $\text{NH}_4\text{Cl}$ . The aqueous layer was extracted with dichloromethane (5  $\times$  30 mL) and the combined organic phases were washed with a saturated aqueous solution of  $\text{NaCl}$  and dried over  $\text{MgSO}_4$ . The solvent was evaporated and the crude yellow solid was purified by column chromatography (eluent: *n*-pentane/dichloromethane 8:1) to give 1,8-bis(phenylethynyl)anthracene as a bright yellow solid. Yield 0.77 g, 41%.  $^1\text{H}$  NMR (500 MHz,  $\text{CDCl}_3$ ):  $\delta = 9.64$  (s, 1H, H9), 8.48 (s, 1H, H10), 8.02 (d,  $^3J_{\text{H,H}} = 8.6$  Hz, 2H, H4/H5), 7.82 (d,  $^3J_{\text{H,H}} = 6.7$  Hz, 2H, H2/H7), 7.60 (m, 4H, *o*-PhH), 7.49 (dd,  $^3J_{\text{H,H}} = 7.1, 8.2$  Hz, 2H, H3/H6), 7.34 (m, 2H, *p*-PhH), 7.22 (m, 4H, *m*-PhH) ppm.  $^{13}\text{C}\{^1\text{H}\}$  NMR (125 MHz,  $\text{CDCl}_3$ ):  $\delta = 131.97, 131.67, 131.59, 130.71, 129.10, 128.56, 128.45, 127.66, 125.34, 124.26, 123.43, 121.63, 95.04, 87.75$  ppm. MS (EI, 70 eV):  $m/z$  [selection, assignment] = 378.1 [ $\text{M}]^+$ , 275.2 [ $\text{M} - \text{C}_8\text{H}_5$ ] $^+$ . HRMS: calculated for  $\text{C}_{30}\text{H}_{18}^+$ : 378.14085, measured: 378.13823.



**Scheme 2** Numbering scheme for a 1,8-substituted anthracene derivative.

**Crystal Structure Determination.** Suitable crystals of the 1,8-bis(phenylethynyl)anthracene were obtained by slow evaporation of saturated solutions of  $\text{CDCl}_3$ . They were selected, coated with paratone-*N* oil, mounted on a glass fiber and transferred onto the goniometer of the diffractometer into a nitrogen gas cold stream solidifying the oil. Data collection was performed on a Bruker *AXS X8 ProspectorUltra* with *APEX II* diffractometer. Empirical formula  $\text{C}_{30}\text{H}_{18}$ ,  $M_r = 378.44$ ,  $\lambda = 1.54178$  Å,  $T = 100(2)$  K,  $F(000) = 2772$ , crystal system monoclinic, space group  $P2_1/n$ ,  $a = 10.898(1)$  Å,  $b = 37.356(2)$  Å,  $c = 17.593(1)$  Å,  $\beta = 99.613(2)^\circ$ ,  $V = 7061.8(5)$  Å<sup>3</sup>,  $Z = 14$ ,  $\rho_{\text{calcd}} = 1.246$  g cm<sup>-3</sup>,  $\mu = 0.537$  mm<sup>-1</sup>,  $\theta_{\text{max}} = 66.85^\circ$ , index ranges  $-12 \leq h \leq 12$ ,  $-41 \leq k \leq 44$ ,  $-19 \leq l \leq 20$ , 53266 reflections collected, 12390 independent reflections,  $R_{\text{int}} = 0.0283$ , 10971 reflections with  $I > 2\sigma(I)$ , 1081 parameters refined. Using the program Olex,<sup>34</sup> the structure was solved by direct methods and refined by full-matrix least-squares cycles (program SHELX-97).<sup>35</sup>  $R$ -values for observed reflections were  $R_1 = 0.0361$ ,  $wR_2 = 0.0923$ , for all reflections  $R_1 = 0.0416$ ,  $wR_2 = 0.0964$ ,  $\text{GoF}$  on  $F^2 = 1.012$ . Max./min. residual electron density was 0.27/−0.34 e Å<sup>-3</sup>. Disorder of C(91) to C(120) on an inversion centre. CCDC 1060040 contains the supplementary crystallographic data for this paper. These data can be obtained free of charge from The Cambridge Crystallographic Data Centre via [www.ccdc.ac.uk/data\\_request/cif](http://www.ccdc.ac.uk/data_request/cif).

**Combined gas electron diffraction / mass-spectrometric experiment.** The combined gas electron diffraction / mass spectrometry (GED/MS) experiment was performed in synchronous mode using the Ivanovo GED/MS apparatus consisting of an EMR-100 GED apparatus and an APDM-1 monopole mass spectrometric unit.<sup>36,37</sup> A sample of 1,8-BPEA was evaporated at a temperature of 498(7) K from a stainless steel (X18H10T) effusion cell with 0.6  $\times$  2.5 mm (diameter  $\times$  length) size for the effusion nozzle. The conditions of (GED/MS) experiments are shown in Table S4.

The gas-phase electron diffraction patterns were scanned by an automated microphotometer<sup>38</sup> at a step of 0.1 mm along the diagonal of the plate. A 10  $\times$  130 mm region was scanned; the number of equidistant scan lines was 33. The total intensity curves were obtained in the ranges  $s = 1.3$ –16.7 Å<sup>-1</sup>;  $\delta = 2.6$ –29.6 Å<sup>-1</sup>.

Simultaneously with recording the electron diffraction patterns, the mass spectra of 1,8-BPEA vapor were recorded. In these the molecular ion  $[\text{C}_{30}\text{H}_{18}]^+$  was the most intensive. Among ions occurring by dissociative ionization by electronic impact of monomer molecule only two ions showed signal with the relative abundance above 15%:  $[\text{C}_{15}\text{H}_9]^+$ , or  $\frac{1}{2}[\text{C}_{30}\text{H}_{18}]^+$  and  $[\text{C}_{15}\text{H}_5]^+$ . No volatile admixtures were detected. It should be noted that there is a satisfactory similarity of ion sets and ion current relative abundances in the mass spectra which had been recorded in two independent experiments ( $L_1 = 598$  mm and  $L_2 = 338$  mm). The masses recorded for 1,8-BPEA are given in Table S5.

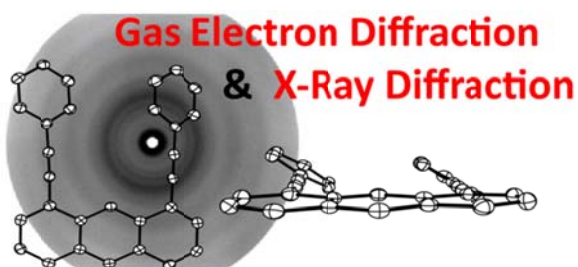
## Acknowledgements

The authors thank Dipl.-Ing. Klaus-Peter Mester for recording NMR spectra as well as Heinz-Werner Patruck for measuring mass spectra. We gratefully acknowledge the Deutsche Forschungsgemeinschaft DFG [grants MI-477/28-1 (SPP1807: Control of London dispersion interactions in molecular chemistry) and MI-477/21-1 (core facility GED@BI)] and the Russian Foundation for Basic Researches for financial support of the Russian-German Cooperation (grants DFG OB 28/22-1 and RFBR 12-03-91333-NNIO\_a) and the Ministry of Education and Science of the Russian Federation (Project Supporting Program, Task No 4.1385.2014K) for financial support of structural analysis computations. We are sincerely grateful to Dr. V. V. Rybkin for fruitful discussions.

## Notes and references

- 1 J. M. Shaw and P. F. Seidler, *IBM J. Res. & Dev.*, 2001, **45**, 3.
- 2 F. Pichierri, *J. Mol. Struct. (Theochem)*, 2004, **686**, 57.
- 3 K. Moor, J. H. Kim, S. Snow and J. H. Kim, *Chem. Commun.*, 2013, **49**, 10829.
- 4 Y. S. Han, S. Jeong, S. C. Ryu, E. J. Park, E. J. Lyu, G. Kwak and L. S. Park, *Mol. Cryst. Liq. Cryst.*, 2009, **513**, 163.
- 5 C. Zhang, Y. Yan, Y. Y. Jing, Q. Shi, Y. S. Zhao and J. Yao, *Adv. Mater.*, 2012, **24**, 1703.
- 6 A. D. Malakhov, M. V. Skorobogatyi, I. A. Prokhorenko, S. V. Gontarev, D. T. Kozhich, D. A. Stetsenko, I. A. Stepanova, Z. O. Shenkarev, Yu. A. Berlin and V. A. Korshun, *Eur. J. Org. Chem.*, 2004, 1298.
- 7 N. N. Dioubankova, A. D. Malakhov, Z. O. Shenkarev and V. A. Korshun, *Tetrahedron*, 2004, **60**, 4617.
- 8 J.-H. Lamm, J. Glatthor, J.-H. Weddelling, A. Mix, J. Chmiel, B. Neumann, H.-G. Stammer and N. W. Mitzel, *Org. Biomol. Chem.*, 2014, **12**, 7355.
- 9 J.-H. Lamm, P. Niermeier, A. Mix, J. Chmiel, B. Neumann, H.-G. Stammer and N. W. Mitzel, *Angew. Chem.*, 2014, **126**, 8072; *Angew. Chem. Int. Ed.*, 2014, **53**, 7938.
- 10 J. Chmiel, B. Neumann, H.-G. Stammer and N. W. Mitzel, *Chem. Eur. J.*, 2010, **16**, 11906.
- 11 M. Goichi, K. Segawa, S. Suzuki, S. Toyota, *Synthesis*, 2005, 2116.
- 12 G. Karlstrom, P. Linse, A. Wallqvist and B. Jonsson, *J. Am. Chem. Soc.*, 1983, **105**, 3777.
- 13 P. Hobza, H. L. Selzle and E. W. Schlag, *J. Phys. Chem.*, 1993, **97**, 3937.
- 14 P. Hobza, H. L. Selzle and E. W. Schlag, *J. Am. Chem. Soc.*, 1994, **116**, 3500.
- 15 R. L. Jaffe and G. D. Smith, *J. Chem. Phys.*, 1996, 105, 2780.
- 16 S. Tsuzuki, T. Uchimarui, M. Mikami and K. Tanabe, *Chem. Phys. Lett.*, 1996, **252**, 206.
- 17 K. C. Janda, J. C. Hemminger, J. S. Winn, S. E. Novick, S. J. Harris and W. Klemperer, *J. Chem. Phys.*, 1975, **63**, 1419.
- 18 J. M. Steed, T. A. Dixon and W. Klemperer, *J. Chem. Phys.*, 1979, **70**, 4940.
- 19 E. Arunan and H. S. Gutowsky, *J. Chem. Phys.*, 1993, **98**, 4294.
- 20 V. A. Ventura and P. M. Felker, *J. Chem. Phys.*, 1993, **99**, 748.
- 21 a) M. O. Sinnokrot and C. D. Sherrill, *J. Phys. Chem. A*, 2004, **108**, 10200; b) M. Schnell, J.-U. Grabow, G. v. Helden, U. Erlekam, P. R. Bunker, G. Meijer and A. van der Avoird, *Angew. Chem.* 2013, **125**, 5288; *Angew. Chem. Int. Ed.* 2013, **52**, 5180.
- 22 S. Grimme, *J. Comput. Chem.*, 2006, **27**, 1787.
- 23 S. Grimme, J. Antony, S. Ehrlich and H. Krieg, *J. Chem. Phys.*, 2010, **132**, 154104-1.
- 24 F. Vögtle, H. Koch, K. Rissanen, *Chem. Ber.*, 1992, **125**, 2129.
- 25 a) A. D. Becke, *J. Chem. Phys.*, 1993, **98**, 5648; b) T. Yanai, D. P. Tew and N. C. Handy, *Chem. Phys. Lett.*, 2004, **393**, 51; c) H. Iikura, T. Tsuneda, T. Yanai and K. Hirao, *J. Chem. Phys.*, 2001, **115**, 3540; d) O. A. Vydrov, G. E. Scuseria and J. P. Perdew, *J. Chem. Phys.*, 2007, **126**, 154109-1; e) Y. Zhao and D. G. Truhlar, *Theor. Chem. Acc.*, 2007, **120**, 215.
- 26 T. H. Dunning, *J. Chem. Phys.*, 1989, **90**, 1007.
- 27 a) V. A. Sipachev, *J. Mol. Struct. (Theochem)*, 1985, **121**, 143; b) V. A. Sipachev, *J. Mol. Struct.*, 2001, **567-568**, 67; c) V. A. Sipachev, *Struct. Chem.*, 2000, **11**, 167.
- 28 a) L. Hedberg and I. M. Mills, *J. Mol. Spectrosc.*, 1993, **160**, 117; b) L. Hedberg and I. M. Mills, *J. Mol. Spectrosc.*, 2000, **203**, 82.
- 29 a) D. A. Wann, R. J. Less, F. Rataboul, P. D. McCaffrey, A. M. Reilly, H. E. Robertson, P. D. Lickiss and D. W. H. Rankin, *Organometallics*, 2008, **27**, 4183; b) D. A. Wann, A. V. Zakharov, A. M. Reilly, P. D. McCaffrey and D. W. H. Rankin, *J. Phys. Chem. A*, 2009, **113**, 9511; c) A. V. Zakharov, Y. V. Vishnevskiy, N. Allefeld, J. Bader, B. Kurscheid, S. Steinhauer, B. Hoge, B. Neumann, H.-G. Stammer, R. J. F. Berger and N. W. Mitzel, *Eur. J. Inorg. Chem.*, 2013, **19**, 3392.
- 30 W. C. Hamilton, *Acta Cryst.*, 1965, **18**, 502.
- 31 J. Emsley, *The Elements*, Oxford University Press, Oxford, 1991, vol. 2.
- 32 Y. Li, J. Zhao, X. Yin, H. Liu, G. Yin, *Phys. Chem. Chem. Phys.*, 2007, **9**, 1186.
- 33 C. Wang, Y. Liu, Z. Ji, E. Wang, R. Li, H. Jiang, Q. Tang, H. Li and W. Hu, *Chem. Mater.*, 2009, **21**, 2840.
- 34 O. V. Dolomanov, L. J. Bourhis, R. J. Gildea, J. A. K. Howard and H. Puschmann, *J. Appl. Crystallogr.*, 2009, **42**, 339.
- 35 G. M. Sheldrick, *Acta Crystallogr. A*, 2008, **64**, 112.
- 36 G. V. Girichev, A. N. Utkin and Yu. F. Revichev, *Prib. Tekh. Eksp.*, 1984, **2**, 187.
- 37 G. V. Girichev, S. A. Shlykov and Yu. F. Revichev, *Prib. Tekh. Eksp.*, 1986, **4**, 167.
- 38 E. G. Girichev, A. V. Zakharov, G. V. Girichev and M. I. Bazanov, *Izv. Vyssh. Uchebn. Zaved., Tekstiln. Prom.*, 2000, **2**, 142.

Entry for the table of contents:



Page No

### 1,8-Bis(phenylethynyl)anthracene – gas and solid phase structures

J.-H. Lamm, J. Horstmann, H.-G. Stammer, N. W. Mitzel,\*  
Yu. A. Zhabanov, N. V. Tverdova, A. A. Otlyotov, N. I. Giricheva  
and G. V. Girichev\*

The structure of 1,8-bis(phenylethynyl)anthracene (1,8-BPEA) has been studied in detail in gas phase and solid state by a combined GED/MS method in synchronous mode and by XRD of a single crystal. Aryl...aryl interactions are discussed in terms mutual repulsion and attraction by dispersive forces.